392 Vol. 38, No. 2 / February 2021 / Journal of the Optical Society of America B Research Article

Journal of the Optical Society of America B

OPTICAL PHYSICS

Emergence of Fano response in trimer structure with asymmetric permittivity

MISAEL NATANAEL,[1] ALEXANDER A. ISKANDAR,[1,*] AND RADIUS N. S. SURYADHARMA[2]

[1]Physics of Magnetism and Photonics Research Division, Faculty of Mathematics and Natural Sciences, Institut Teknologi Bandung, Jl. Ganesa 10, Bandung 40132, Indonesia

[2]Laser Physics and Nonlinear Optics Group, Faculty of Science and Technology, MESA+ Institute for Nanotechnology, University of Twente, Enschede, The Netherlands

*Corresponding author: iskandar@fi.itb.ac.id

Received 29 September 2020; revised 4 December 2020; accepted 8 December 2020; posted 9 December 2020 (Doc. ID 410680); published 11 January 2021

In this paper, we discuss the Fano response from a hybrid trimer composed of gold and silicon nanospheres. This allows the structure to exhibit plasmonic properties while having a versatile spectral tuning of its Fano response. We analyze the Fano response from the point of view of the individual subsystem as well as the coupling of supermodes of the structure. The coupling between the sustained non-orthogonal eigenmodes can be traced as a result of these modes sharing the same multipolar moments. With this, we provide insight into designing a hybrid structure with tunable Fano properties.

https://doi.org/10.1364/JOSAB.410680

1. INTRODUCTION

Fano resonances have attracted much interest in optics due to their asymmetric lineshapes, which often exhibit very sharp spectral features [1–3]. Based on their sharp spectral responses, multiple applications exploiting Fano resonances have been proposed. Examples of these applications are optical switches [4–6] and optical sensing devices [7–10]. On the other hand, the near-field properties of Fano resonances around the scatterer can also be used to enhance several observable quantities, such as Raman scattering [11,12], nonlinear response [13,14], circular dichroism [15,16], or scattering suppression [17].

The origin of Fano resonance is often explained in terms of spectral interference between different modes supported by the scatterer [1,2]. For a specific incident field, several modes are usually excited simultaneously in the scatterer. If some of the excited modes are nonorthogonal to each other, a cross-coupling between them occurs. This effect manifests itself in the form of constructive or destructive interference, which can be measured from spectrally observable quantities. For the simplest case involving two nonorthogonal modes, the mode that is spectrally broader (weaker dispersion) than the other one is called the bright mode, while the mode with a narrower spectral response exhibiting rather strong dispersion in its spectral phase is called the dark mode. The interference between these two modes results in a sharp spectral response of the scatterer. The most prominent example of a system whose spectral response can be fully analyzed by such an argument is the dolmen structure [18,19].

On the other hand, many scatterers often consist of large amounts of particles [20–22]. In this case, identifying relevant modes can be challenging. This complication arises because the properties of these scatterers cannot be explained simply in terms of modes supported by each constituent, but rather as supermodes of interacting particles [23]. These supermodes depend strongly on the arrangement and the optical properties of each individual particle. For this particular reason, in contrast to the interaction of eigenmodes of the isolated subsystem as discussed before, here the collective eigenmodes of the entire structure are used to explain Fano features arising from a scatterer consisting of many particles [24,25]. Because this description relies on collective modes supported by the structure, their identification is the most important requirement to understand the feature of Fano resonance that arises from such a structure.

In this work, using the eigenmode description from the T-matrix, we investigate the emergence of Fano response in a trimer scatterer system that consists of gold nanosphere(s) coupled to silicon nanosphere(s). The sphere is chosen as a basic building block, as it represents a structure that can be fabricated easily via a bottom-up approach [26,27]. We chose this hybrid system because it possesses flexible tunability of the response of silicon nanospheres and the plasmonic behavior of gold nanoparticles. We show that the scattering cross section can be decomposed into terms that come from the contribution of each individual eigenmode and from the coupling contribution of the sustained nonorthogonal eigenmodes. Further investigation shows that these couplings originate from the fact that the

involved eigenmodes share the same multipole components. With these results, we provide insight into designing a hybrid structure that provides a Fano response, which can be useful for many applications.

2. T-MATRIX FORMULATION FOR MULTIPARTICLE SYSTEM

When dealing with scattering problems, the fields are usually decomposed into an orthogonal basis set. In our case, we choose vector spherical harmonics (VSH) as our preferential basis set due to the fact that it is quite straightforward to extract multipole information, which we will use extensively later on. Here, the incident ($\mathbf{E}_i$) and scattered fields ($\mathbf{E}_s$) of a scatterer can be expanded in VSH, written as

$$\mathbf{E}_i = \sum_{n=1}^{\infty}\sum_{m=-n}^{n}[p_{mn}\mathbf{N}_{mn}^{(1)} + q_{mn}\mathbf{M}_{mn}^{(1)}], \tag{1a}$$

$$\mathbf{E}_s = \sum_{n=1}^{\infty}\sum_{m=-n}^{n}[a_{mn}\mathbf{N}_{mn}^{(3)} + b_{mn}\mathbf{M}_{mn}^{(3)}]. \tag{1b}$$

Here, $\mathbf{M}_{mn}$ and $\mathbf{N}_{mn}$ are VSH [28], (p_{mn}, q_{mn}) denote the expansion coefficients of the incident field, and (a_{mn}, b_{mn}) denote the expansion coefficients of the scattered field. The superscript on VSH denotes the type of Bessel function being used: (1) for a spherical Bessel function of the first kind j_n or (3) for a spherical Hankel function of the first kind $h_n^{(1)}$. In practical computation, the summation over n must be terminated at some value $n = N_B$, which correlates to the amount of VSH used in the expansion. In our calculation, we use $N_B = 4$, which yields an error less than 1% over the region of interest. From these expansion coefficients, we can extract the multipole field contributions [29], specifically, the a_{mn} coefficients are associated with the electric multipoles, and the b_{mn} coefficients are associated with the magnetic multipoles; $n = 1$ refers to the dipole contribution, $n = 2$ refers to the quadrupole contribution, and so on.

To link the scattered and incident field coefficients, T-matrix formulation can be used. It reads as

$$\begin{pmatrix} T_{11} & T_{12} \\ T_{21} & T_{22} \end{pmatrix}\begin{pmatrix} p_{mn} \\ q_{mn} \end{pmatrix} = \begin{pmatrix} a_{mn} \\ b_{mn} \end{pmatrix}. \tag{2}$$

Here, T_{11}, T_{12}, T_{21}, and T_{22} are submatrices of the T-matrix of the system being considered. The T-matrix depends only on the geometry and configuration of the scatterer and is independent of the incident field [28]. To obtain the T-matrix of the system, several numerical methods can be employed. For a single sphere, the associated T-matrix takes a very simple form, which is a diagonal matrix. The diagonal components are the corresponding Mie coefficients (a_n, b_n) of the respective sphere [30,31]. For an arbitrary scatterer, the T-matrix can also be obtained as shown in [32–34].

In a multiparticle system, there are two coordinates that can be employed for T-matrix formulation: local coordinates of each individual particle and global coordinates that represent the whole system [35]. Every field in each local coordinate has different expansion coefficients. Consider a system consisting of N particles. In local coordinate formulation, the incident field on particle j ($\mathbf{E}_i^j$) can be separated into two parts: external field from a source and scattered fields from the other particles in the system. This can be stated mathematically as

$$\mathbf{E}_i^j = \mathbf{E}_0^j + \sum_{l\neq j}^{N}\mathbf{E}_s^{l,j}. \tag{3}$$

The first term of Eq. (3) denotes the external incident field from the source in the referential frame of local coordinate j. The expansion coefficients of this field will be notated as (p_{mn}^j, q_{mn}^j). The second term describes the scattered field from particle l to particle j. To evaluate this term, an addition theorem of VSH must be employed to transform fields from one local coordinate of the scatterer to the other local coordinates of different scatterers. The translation of the fields means that the VSH in one local coordinate are expanded into VSH in another local coordinate [36,37]. Transforming a scattered field from particle l into an incident field for particle j can be expressed as

$$\mathbf{M}_{mn}^{(1)}(j) = \sum_{n=1}^{\infty}\sum_{m=-n}^{n}[A_{mn}^{\mu\nu}(l,j)\mathbf{M}_{\mu\nu}^{(3)}(l) + B_{mn}^{\mu\nu}(l,j)\mathbf{N}_{\mu\nu}^{(3)}(l)], \tag{4a}$$

$$\mathbf{N}_{mn}^{(1)}(j) = \sum_{n=1}^{\infty}\sum_{m=-n}^{n}[B_{mn}^{\mu\nu}(l,j)\mathbf{M}_{\mu\nu}^{(3)}(l) + A_{mn}^{\mu\nu}(l,j)\mathbf{N}_{\mu\nu}^{(3)}(l)], \tag{4b}$$

where $A_{mn}^{\mu\nu}(l,j)$ and $B_{mn}^{\mu\nu}(l,j)$ represent the translation coefficient from coordinate l to j [38]. Employing Eq. (4) in Eq. (3), we obtain

$$P_{mn}^j = p_{mn}^j - \sum_{l\neq j}^{N}\sum_{\nu=1}^{\infty}\sum_{\mu=-\nu}^{\nu}[a_{\mu\nu}^l A_{mn}^{\mu\nu}(l,j) + b_{\mu\nu}^l B_{mn}^{\mu\nu}(l,j)], \tag{5a}$$

$$Q_{mn}^j = q_{mn}^j - \sum_{l\neq j}^{N}\sum_{\nu=1}^{\infty}\sum_{\mu=-\nu}^{\nu}[a_{\mu\nu}^l B_{mn}^{\mu\nu}(l,j) + b_{\mu\nu}^l A_{mn}^{\mu\nu}(l,j), \tag{5b}$$

where (P_{mn}^j, Q_{mn}^j) denote the expansion coefficients of the total incident field of particle j, and $(a_{\mu\nu}^l, b_{\mu\nu}^l)$ denote the expansion coefficients of the scattered field of particle l. These coefficients can be linked via T-matrix formulation of the system in local coordinates, T_{local}, as

$$T_{\text{local}}\begin{pmatrix} P_{mn}^j \\ Q_{mn}^j \end{pmatrix} = \begin{pmatrix} a_{mn}^j \\ b_{mn}^j \end{pmatrix}. \tag{6}$$

Using Eq. (6), the scattered field from each individual particle can be obtained.

To obtain the T-matrix in global coordinates, we have to choose a single point in space as the referential global coordinate origin. In principle, there are no rules for choosing this point, so it can be any arbitrary point in space. Nevertheless, choosing a referential point too far from the system requires higher N_B for the infinite summation to be converged. Choosing a symmetric point of the system as the global origin usually helps to keep N_B

as low as possible [39]. After choosing the global origin of the system, the total scattered fields from local coordinates of each individual particle have to be translated into the chosen global coordinate system. Furthermore, the external incident field from the source has to be translated from global coordinates into local coordinates of each particle [40,41]. The need for these transformations will become more transparent in its use in T-matrix transformation. In matrix notation, we obtain the T-matrix of the system in global coordinates, T_{global}, by transforming the T-matrix in local coordinates as

$$T_{\text{global}} = W T_{\text{local}} V, \tag{7}$$

where W denotes the translation coefficient matrix from local to global coordinates, and V is the same matrix as W but consists of translation from global to local coordinates.

3. EXTRACTING EIGENMODES FROM THE *T*-MATRIX

Scattering eigenmodes from the system can be extracted using eigenvalue decomposition (EVD) to the T-matrix. This can be stated as

$$T = XEX^{-1}, \tag{8}$$

where X is a matrix whose columns are the eigenvectors of T, and E is the diagonal matrix that stores the eigenvalues η of the matrix T. We can use either T_{local} or T_{global} for the matrix T. Here, we will use global formulation for mode analysis due to the reduced number of involved modes compared to local formulation.

One of the most common observable quantities used to describe scattering characteristics from a system is the scattering cross section C_{sca}. To calculate C_{sca}, the summation is performed over the absolute square of the scattering coefficient (a_{mn}, b_{mn}) [42] associated with individual VSH. In eigenmode analysis, C_{sca} can be decomposed in terms of modes obtained from the T-matrix [35]. Using global coordinates formulation, the decomposition of C_{sca} yields

$$C_{\text{sca}} = \frac{4\pi}{k^2} \sum_j \sum_i \eta_i \eta_j^* \langle p|y_j\rangle \langle y_i|p\rangle \langle x_j|x_i\rangle. \tag{9}$$

Here, k is the wavenumber of light, $|p\rangle$ refer to coefficients of external incident field, $|x_i\rangle$ denotes the eigenvector associated with eigenmode i, and $|y_i\rangle$ denotes the eigenvectors of the Hermitian conjugate of T, $T^\dagger$. Further, we can separate the above summation into direct $(i = j)$ and interference $(i \neq j)$ terms to yield

$$C_{\text{sca}} = C_{\text{direct}} + C_{\text{interference}}. \tag{10}$$

The first term of Eq. (10) corresponds to the contribution from eigenmodes i, while the second term corresponds to the interference between eigenmodes i and j. This term arises whenever nonorthogonal modes exist and are excited simultaneously. This interference term is the source of the emergence of Fano resonance in the system [25]. Note that this interference term contains dependency on the incident field as denoted in Eq. (9). This implies that the Fano properties depend heavily on the incident field. For example, when discussing Fano properties arising from different polarizations, the contribution of the excited eigenmodes and their cross-coupling can be analyzed directly.

The decomposition of the T-matrix is done independently for each wavelength. Hence, the eigenmodes for each wavelength have to be ordered in a distinct way. To sort the eigenmodes in a proper way, we use a sorting algorithm as described in [43]. This algorithm computes eigenvalues and eigenvectors for each wavelength while maintaining order in a consistent manner.

4. GOLD–SILICON TRIMER STRUCTURE

In this paper, we chose a trimer, as it constitutes a rather simple structure that supports Fano resonance [44]. Here, we take silicon as one component of the main building block instead of a trimer, which is composed of three gold nanospheres due to the tunability of the response of the silicon nanosphere, allowing a flexible detuning of the frequency of one of the components. Consider the case of a single gold nanosphere; a small resonance peak shift, around 10 nm, can be observed when the radius of the nanosphere changes from 70 nm to 75 nm and from 75 nm to 80 nm [Fig. 1(a)]. On the other hand, for the same size of change, the silicon nanosphere resonance peak shifts more

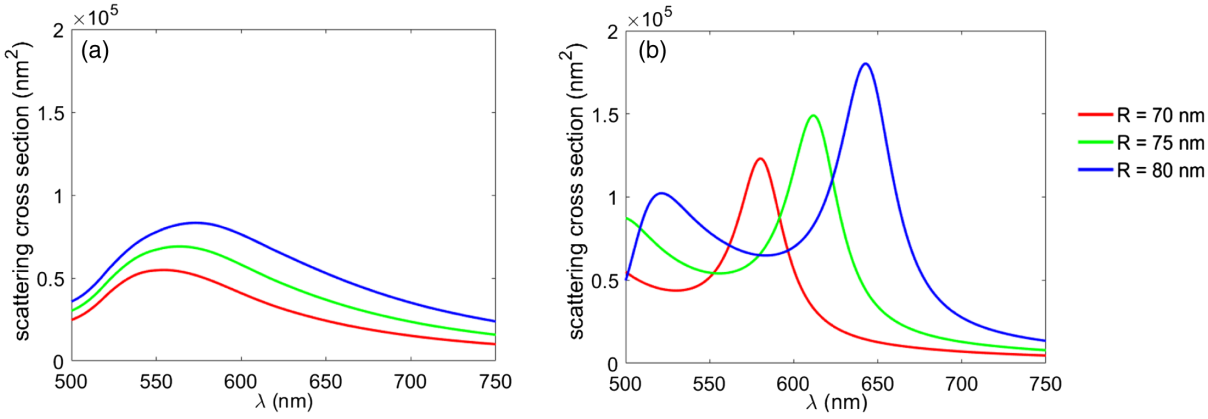

Fig. 1. Scattering cross section from a single (a) gold nanosphere and (b) silicon nanosphere embedded in vacuum with various radius sizes. Different resonance shift behavior between silicon and gold nanospheres is observed.

noticeably around 30 nm [Fig. 1(b)]. This shows that a silicon nanosphere exhibits a more sensitive response compared to a gold nanosphere, therefore showing its superior tunability compared to the gold nanosphere.

In this paper, we assume that our structure is embedded in air, $n_b = 1$. Experimental data of the refractive index from Johnson–Christy [45] and Aspnes–Studna [46] are used for gold and silicon calculations, respectively. To understand the effect of the coupling between two subsystems, it is desirable to understand the response of each individual subsystem. For our case, we want to design the gold dimer to support the magnetic dipole (MD) mode, which will be coupled to the mode supported by the silicon sphere later on. We keep the size of an individual sphere big enough such that it is comparable to the size of the silicon nanosphere that will be introduced later on. We choose the radius of the gold nanosphere to be 100 nm. The scattering response and its decomposition into its multipolar components are shown in Fig. 2(a). Here, we observe that for a single gold nanosphere, the response consists mainly of the electric dipole (ED) contribution, which resonates at 615 nm, and a much smaller electric quadrupole (EQ) contribution, which resonates at 522 nm. Dimer structure is chosen such that the MD mode in global coordinates has well-pronounced strength. For this purpose, we choose center-to-center distance between the two gold nanospheres to be around half of the wavelength of the resonance wavelength of the ED mode of a single sphere. Here, 280 nm center-to-center distance is chosen, which translates into 80 nm surface-to-surface distance. This allows an out-of-phase response of each individual gold nanoparticle via plane wave excitation, therefore forming a MD mode in the global coordinate centered at the center of mass of the two-sphere system. Figure 2(b) shows the multipolar decomposition of the scattering cross section with the incident field direction and polarization denoted in the inset. Here, two dominant modes are observed, MD and EQ modes. The MD is the direct result of the design strategy mentioned before. In the center coordinate system, the EQ appears due to the ED's arrangement. The ED response of the total system, however, is suppressed considerably due to this out-of-phase response of individual spheres.

The second subsystem that needs to be designed is the silicon nanosphere. The size of silicon nanospheres should be big enough to support resonance of a dipole mode. The response of the silicon nanosphere with a radius R_s is chosen such that the resonance peak happens to be slightly detuned from the resonance of the gold dimer structure, resulting in $R_s = 75$ nm. The decomposition of scattering response into its multipolar compositions of this silicon nanosphere can be seen in Fig. 2(c). Here, a pronounced MD mode appears around 630 nm, which is slightly blue shifted more than the mode resonance frequencies of the gold dimer. Finally, we couple these two subsystems by placing the silicon nanosphere such that it forms an equilateral triangle with the distance to the gold dimer structure $d_2 = 55$ nm. The structure is illuminated by a plane wave with its polarization and propagation vector of incident wave all in-plane to allow the efficient excitation of the MD mode of the gold dimer structure. This incident field will also excite the MD mode of the silicon nanosphere, therefore allowing mode coupling and, consequently, the emergence of a Fano profile.

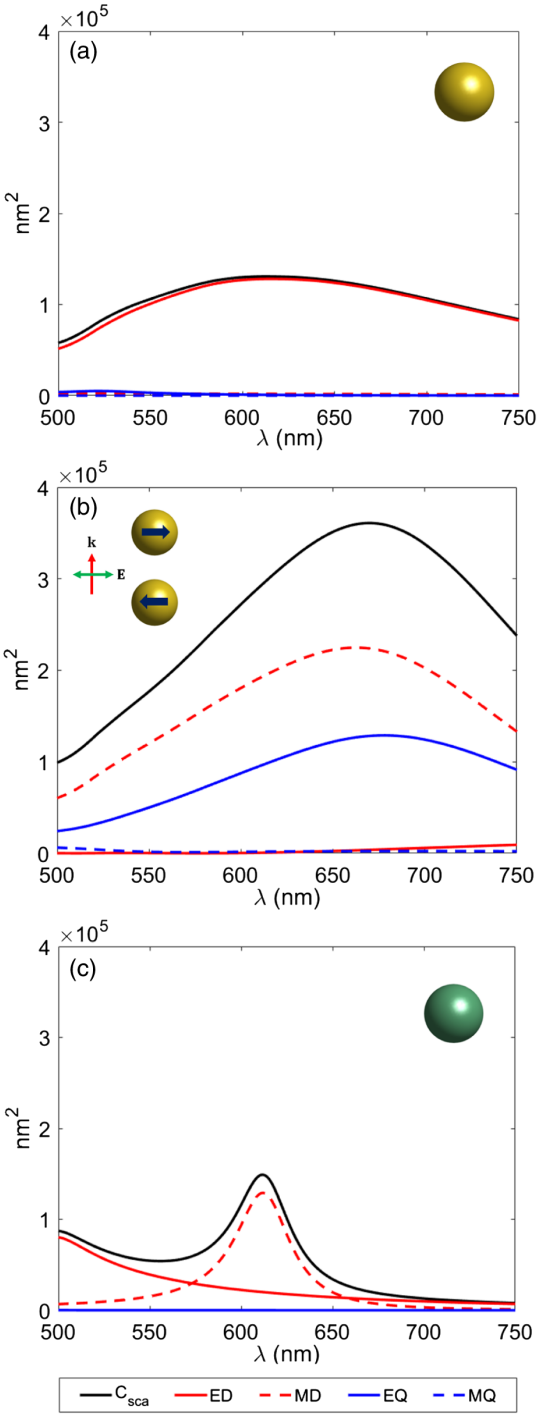

Fig. 2. Multipolar decomposition of the scattering cross section of (a) single gold sphere, (b) gold dimer, and (c) single silicon sphere, which can be regarded as subsystems of the structure being considered in Fig. 3. Shown here are the electric dipole (ED), magnetic dipole (MD), electric quadrupole (EQ), and magnetic quadrupole (MQ) contribution to the cross section.

The schematic of the resulted structure as well as the incident field scenario are depicted in Fig. 3.

To allow a more quantitative analysis of the origin of the Fano response in our trimer structure, we treat the gold dimer and silicon nanosphere as a whole system. The eigenmodes of

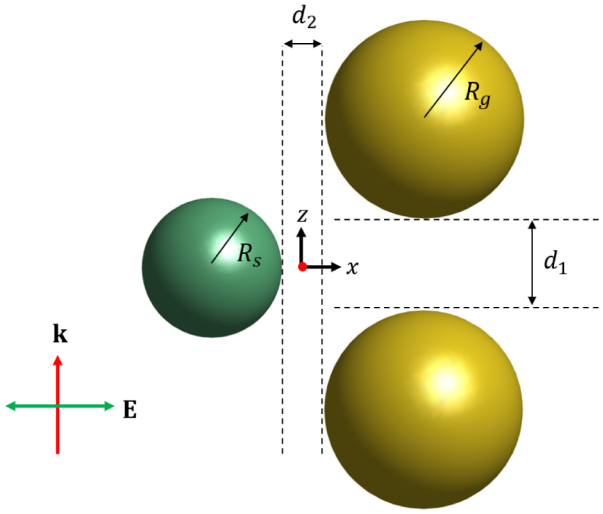

Fig. 3. Structure being considered consists of gold dimer of radius $R_g = 100$ nm with separation $d_1 = 80$ nm and single silicon nanosphere of radius $R_s = 75$ nm. The surface-to-surface distance between the silicon nanosphere and the dimer is $d_2 = 55$ nm. The structure, polarization, and propagation vector of incident wave are all in-plane. The origin of the global coordinates is denoted by the red dot, along with the direction of its associated coordinate axis.

this system are then calculated according to Eq. (8). Figure 4 shows the scattering cross section of the trimer structure with the incident field as depicted in Fig. 3. Here, we decompose the scattering cross section in terms of the contribution of the eigenmodes and their cross-coupling terms. From the scattering cross section spectrum of the trimer structure, we notice two slightly perceptible Fano responses. Close-ups of the scattering cross section spectra around 611 nm and 508 nm are shown in Fig. 4(a) and Fig. 4(b), respectively, along with their dominant eigenmode contributions (solid line) and dominant interference terms (dashed line). The full spectra of the cross section are shown as insets in each figure. A detailed modal analysis will be focused around these two wavelengths, since the interference between the excited eigenmodes occurred there.

The interference terms observed in the trimer structure can be analyzed qualitatively via eigenmodes supported by its individual subsystem. To do this, we inspect its subsystem response, which consists of a gold dimer and single silicon structure. According to the resonance position of each individual component. as shown in Figs. 2(b) and 2(c), we observe that the interference term around 611 nm is the result of the coupling between the MD mode of a silicon nanophere and MD or EQ modes of the gold dimer. On the other hand, interference around 508 nm, which has a larger magnitude, corresponds to the coupling between the ED mode of the silicon nanosphere and MD or EQ modes of the gold dimer. The larger magnitude of this interference term can be attributed to the corresponding multipole mode coupling of the silicon. Since the interaction between two ED modes is much stronger than the interaction between two MD modes (as demonstrated in [47]), we can expect a stronger coupling between the silicon nanosphere and gold dimer around a wavelength with a dominant ED mode. This strong ED coupling results in a larger interference magnitude observed around 508 nm.

On the other hand, we can also describe the magnitude of the coupling in a global coordinates picture, which are obtained from the EVD of the T-matrix in global coordinates. By inspecting the close-up view of the spectra at around 611 nm in Fig. 4(a), we observe three dominant eigenmodes (modes 1, 2, and 6). All of these modes are nonorthogonal to each other, which results in three interference terms. Interference terms between modes 1 and 6 and modes 2 and 6 have more or less the same magnitude with a negative sign, while the coupling between modes 1 and 2 has a positive sign. The summation over these interference terms yields a negative total interference term around 611 nm. The same analysis can be employed for the interference around 508 nm by identifying the eigenmodes and their coupling, as depicted in Fig. 4(b). Around this wavelength, we have all dominant eigenmodes of the system except mode 6. We observe that the three involved interference terms are destructive interference, as shown by their negative contribution to the scattering cross section.

As previously mentioned, interference terms are the products of the coupling between nonorthogonal eigenmodes.

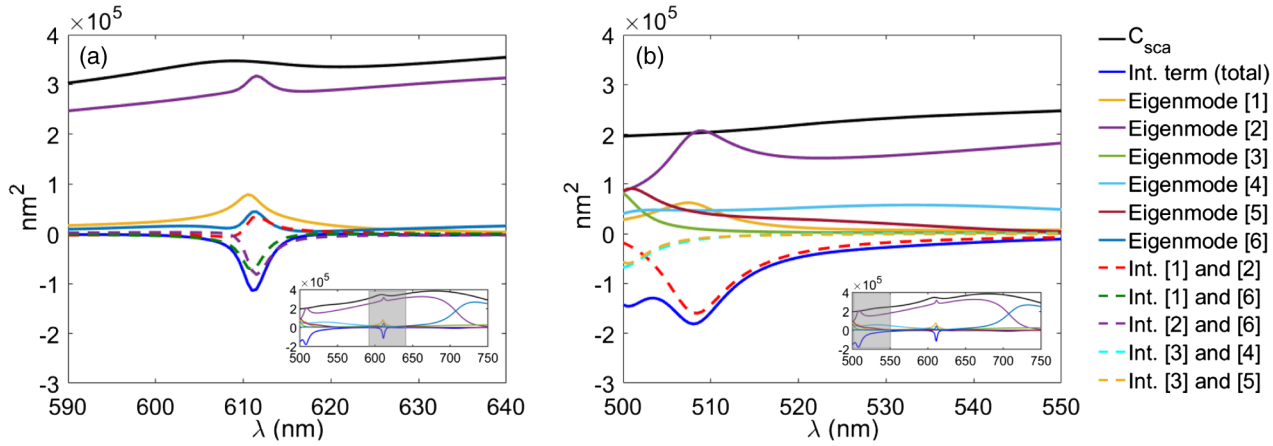

Fig. 4. Close-up view of scattering cross section (black solid line) spectra for the system depicted in Fig. 3 at around (a) 611 nm and (b) 508 nm along with its dominant eigenmodes (solid line) and dominant interference terms (dashed line). The full-wavelength spectra are shown as an inset in each figure. Total interference term is also shown (blue solid line).

Table 1. Contribution of Multipolar Moments in Each Eigenmode at Wavelength of 611 nm

Eigenmode	Multipolar Components
1	$71\%P_z + 24\%M_y + 4\%Q_{xz}$
2	$3\%P_z + 97\%M_y$
3	$94\%P_x + 4\%Q_{zz}$
4	$97\%P_x + 1\%Q_{xx}$
5	$99\%P_x$
6	$76\%P_z + 24\%M_y$

Table 2. Contribution of Multipolar Moments in Each Eigenmode at Wavelength of 508 nm

Eigenmode	Multipolar Components
1	$98\%M_y$
2	$20\%P_z + 78\%M_y$
3	$91\%P_x + 2\%Q_{xx} + 6\%Q_{zz}$
4	$99\%P_x$
5	$46\%P_x + 30\%Q_{xx} + 20\%Q_{yy}$
6	$62\%P_z + 38\%M_y$

This nonorthogonality between eigenmodes can be explained by noting that the corresponding eigenmodes share the same multipolar moments. For example, consider the interference dip at 611 nm. Each eigenmode can be decomposed into its multipolar components. Here, we consider the contributions up to EQ moments. Table 1 shows the normalized contribution of multipolar components for each eigenmode. Decomposition was done using the procedure as stated in [48] as

$$\begin{pmatrix} P_x \\ P_y \\ P_z \end{pmatrix} = \begin{pmatrix} a_{1,1} - a_{1,-1} \\ i(a_{1,1} + a_{1,-1}) \\ -\sqrt{2}a_{1,0} \end{pmatrix}, \tag{11a}$$

$$\begin{pmatrix} Q_{xx} & Q_{xy} & Q_{xz} \\ Q_{yx} & Q_{yy} & Q_{yz} \\ Q_{zx} & Q_{zy} & Q_{zz} \end{pmatrix} = \frac{1}{6\sqrt{5}} \begin{pmatrix} i(a_{2,2} + a_{2,-2}) - \frac{i\sqrt{6}}{2}a_{2,0} & a_{2,-2} - a_{2,2} & i(a_{2,-1} - a_{2,1}) \\ a_{2,-2} - a_{2,2} & -i(a_{2,2} + a_{2,-2}) - \frac{i\sqrt{6}}{2}a_{2,0} & a_{2,-1} + a_{2,1} \\ i(a_{2,-1} - a_{2,1}) & a_{2,-1} + a_{2,1} & i\sqrt{6}a_{2,0} \end{pmatrix}, \tag{11b}$$

where P and Q denote the ED and quadrupole components, respectively. To calculate the magnetic components, the a_{mn} coefficients in Eq. (11) should be replaced by the b_{mn} coefficients, while the expression remains the same.

In Table 1, we can see that modes 1, 2, and 6 share the same ED (P_z) and MD (M_y) moments, where the coordinate system used can be seen in Fig. 3. This results in nonorthogonality between these modes. Hence, each pair of these three eigenmodes contributes to interference terms, as can be seen in Fig. 4. The same analysis can be employed for the interference terms around 508 nm, as can be seen in Table 2. However, it should be stressed that when two or more eigenmodes are nonorthogonal, the nonorthogonality is a direct result of the fact that the involved eigenmodes share the same multipolar moments. It should be noted that the inverse is not always true. Several eigenmodes can share the same multipolar moments, but they can be orthogonal to each other if the phases of the shared multipolar components cancel each other. This fact can be seen from the multipolar decomposition of eigenmodes 3 and 4 at the 611 nm resonance and decomposition of eigenmodes 2 and 6 at the 508 nm resonance.

We have seen that a trimer structure consisting of gold dimer and a single silicon nanosphere can produce interference terms, which results in the observation of the Fano profile in cross section spectra. Next, we will show that using the same trimer geometry but with the materials permittivity swapped (now the structure consists of a silicon dimer of radius 100 nm and single gold nanosphere of radius 75 nm), a Fano profile can also be observed due to interference between nonorthogonal modes. This is additional example of the emergence of a Fano profile in a hybrid metal–dielectric structure. In the following, we will show the design consideration of this inversed-material trimer structure leading to a Fano response that is a result of nonorthogonal eigenmode coupling. As the same analysis presented previously can also be applied in this additional system, for the following discussion, we will extract only a summary of the analysis for the considered structure.

To gain first insight into our inversed-material trimer structure, we will consider the silicon dimer and single gold nanosphere separately as we have done previously. Figure 5 shows the scattering cross section of a trimer structure composed of a silicon dimer and a single gold nanosphere and its decomposition into its multipolar components. The scattering cross section of the gold nanopshere consists of only an ED response. This is because the size of the gold nanosphere is relatively small compared to the wavelength of interest; therefore, it supports only the ED mode. On the other hand, the silicon dimer exhibits several multipolar responses, up to octupole [electric octupole (EO) and magnetic octupole (MO)] terms, which can be seen clearly at around 570 nm for MO. These higher multipole responses are a direct result of coupling between each silicon sphere in the dimer structure. Due to the large size of the silicon (100 nm in this case), the quadrupolar response will be excited. Coupling between these quadrupolar modes can lead to an octupolar response from the global coordinate centered at the center of mass of the system. In Fig. 5, it can be seen that the resonance wavelength of the excited MD mode and MO mode of the silicon dimer are quite close to the resonance wavelength of the ED mode of the gold nanosphere. This strong spectral overlap around the resonance peaks will result in the coupling between these excited modes; therefore, we expect that the Fano response will appear in this spectral range of interest.

Now we will identify the corresponding eigenmodes produced by the inversed-material trimer structure. In this analysis, the silicon dimer and gold nanosphere are treated as one system. We use the same spatial configuration and incident wave orientation as in Fig. 3. Figure 6 shows the scattering cross section (solid black line) of the inversed trimer structure along with its seven dominant eigenmodes' contribution. Also shown are the total interference terms (blue solid line) that result from coupling between nonorthogonal modes.

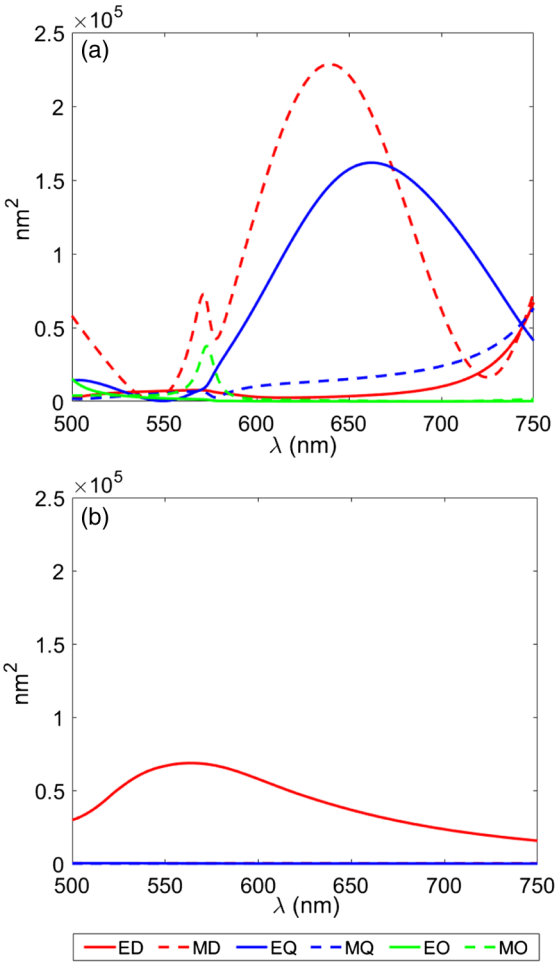

Fig. 5. Multipolar decomposition of the scattering cross section of the (a) silicon dimer and (b) single gold nanosphere, which can be regarded as subsystems of the inversed-material structure in Fig. 3. Here, we show the electric dipole (ED), magnetic dipole (MD), electric quadrupole (EQ), magnetic quadrupole (MQ), electric octupole (EO), and magnetic octupole (MO) contribution to the cross section.

As can be expected, interference terms are produced in the interval between 550 and 600 nm, as seen in Fig. 6. This confirms our qualitative analysis based on the optical response of each subsystem. A Fano profile in the scattering cross section spectra can be observed at around 570 nm. The interference terms in the interval 550–600 nm are rather complicated due to many multipole resonances from the silicon dimer at this wavelength interval [Fig. 5(a)]. Note also the appearance of another interference term with a small magnitude at around 680 nm. Identification of the interference between each eigenmode can be done using the same procedure as employed in the previous trimer structure.

Another analysis can be conducted regarding the tuning aspect of our hybrid trimer structure. Here, we do some variation on the system parameters and observe whether there are any significant changes to the Fano profile. Here, we focus our variation on the first proposed trimer structure (gold dimer and single silicon nanosphere), which will give insight into the underlying physical mechanism related to the tunability of Fano properties in general. The parameters that can be varied are the distance d_1, d_2 and the polarization of the incident field. In our previous case, we chose to fix the incident field polarization to be able to generate a specific multipole mode of interest (MD to be precise) on the gold dimer structure. Therefore, we do variations only on the d_1 and d_2 parameters. This analysis would be beneficial for structural design from an experimental aspect.

Tables 3 and 4 show the information corresponding to the Fano properties of the trimer structure for each variation of d_1 and d_2. To compare the strength of the interference between different structures, we use the ratio of the interference term to the scattering cross section ($C_{\text{int}}/C_{\text{sca}}$). We call this parameter the Fano strength ratio. Here, we measure the difference in this parameter relative to our structure presented in Fig. 3. All quantities presented here are calculated at the Fano resonance wavelength that happens around 611 nm. In Tables 3 and 4, we can see that as d_1 decreases, both C_{sca} and C_{int} increase. On the other hand, as d_2 decreases, both C_{sca} and C_{int} also decrease. Note that this monotonous behavior does not necessarily apply in other variation ranges. The behavior of the interference term with respect to d_1 (which is surface-to-surface distance between gold dimers) variation can be explained as follows. As the distance between two subsystems decreases, the ED contribution of the cross section (red line in Fig. 2) tends to shift to the lower wavelength. This blueshift of the resonance frequency means

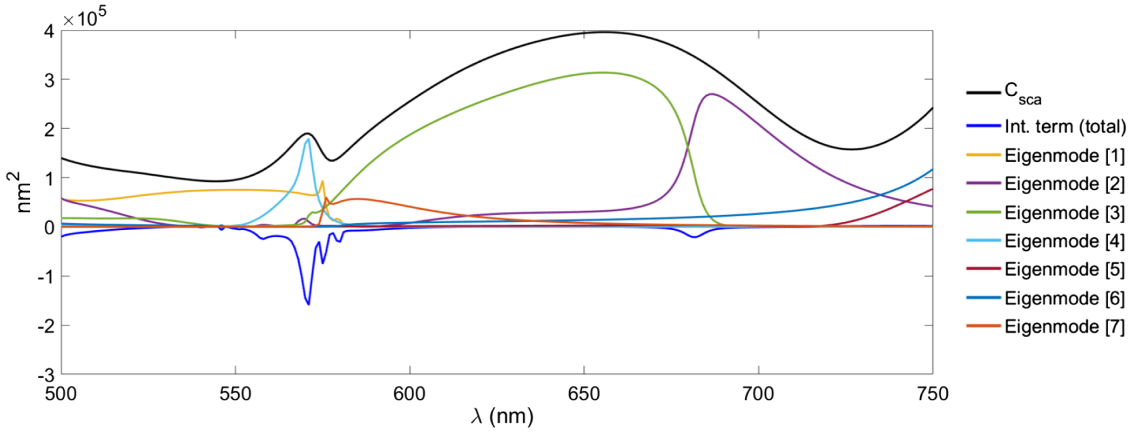

Fig. 6. Scattering cross section spectra (solid black line) for the inversed-material trimer structure along with its seven dominant eigenmodes contribution and total interference terms (solid blue line). Primary interference terms are observed between 550 nm and 600 nm.

Table 3. Difference between the Ratio of the Interference Term (C_{int}) Relative to the Scattering Cross Section (C_{sca}) for Each Variation of d_1[a]

d_1 (nm)	C_{sca} (nm^2)	C_{int} (nm^2)	$\Delta\left(\frac{C_{int}}{C_{sca}}\right)$
60	3.61×10^5	1.88×10^5	0.191
70	3.53×10^5	1.30×10^5	0.038
80	3.46×10^5	1.14×10^5	0
90	3.38×10^5	9.90×10^4	−0.037
100	3.32×10^5	9.64×10^4	−0.040

[a]Differences are relative to default value $d_1 = 80$ nm.

Table 4. Difference between the Ratio of the Interference Term (C_{int}) Relative to the Scattering Cross Section (C_{sca}) for Each Variation of d_2[a]

d_2 (nm)	C_{sca} (nm^2)	C_{int} (nm^2)	$\Delta\left(\frac{C_{int}}{C_{sca}}\right)$
45	3.37×10^5	1.82×10^4	−0.276
50	3.41×10^5	4.79×10^4	−0.189
55	3.46×10^5	1.14×10^5	0
60	3.50×10^5	2.09×10^5	0.267
65	3.54×10^5	4.49×10^5	0.936

[a]Differences are calculated relative to the default value $d_2 = 55$ nm.

there is a stronger scattered field from ED of the dimer at a wavelength of 611 nm. This will result in higher coupling with the silicon nanosphere modes, hence increasing the interference term. The behavior of the interference term with respect to d_2 [which is the distance between the silicon nanosphere and the gold dimer as depicted in Fig. (3)] variation can be associated with the fact that decreasing the surface distance can lead to a partially destructive phase between the interacting modes, hence decreasing the total amount of the interference term. If we compare the results between the variation of d_1 and d_2 for the relative Fano strength ratio ($\Delta(C_{int}/C_{sca})$), it can be inferred that changing d_2 yields a more significant difference in the Fano strength ratio compared to changing d_1. Therefore, within this variation range, d_2 is more sensitive than d_1. The same argument can be applied to different structures as well. Note that changing d_2 generally exhibits a delicate interplay between the phase and amplitude of the scattered field of one subsystem as experienced by the other subsystem.

5. CONCLUSION

In this paper, we have shown that using a hybrid structure allows versatile tuning of the response of individual subsystems to yield a desired Fano response of the whole system. We study a trimer system with different materials (metal and dielectric) and show that this structure can produce a Fano profile in the scattering cross section spectra. Here, we use a gold dimer and single silicon nanosphere as the primary structure of interest. The resulting Fano resonance can be explained as a result of the interference between nonorthogonal eigenmodes in the structure. The design analysis has been done qualitatively by inspecting the optical response of each individual subsystem (dimer and single nanosphere). For a more quantitative identification of the eigenmodes, we employ EVD of the T-matrix of the system in global coordinates. By using this method, interference between eigenmodes is observed. We have shown that the nonorthogonality between eigenmodes is the direct result of the involved modes sharing the same multipolar decomposition. We also show that the inversed-material of the primary structure (silicon dimer and single gold nanosphere) can also produce a Fano profile, and the same analysis procedure can be employed to this structure. By changing the distance between subsystems, the Fano profile can be tuned by the interplay between phase and amplitude of the scattered field from one subsystem as experienced by the other subsystem. With this, we provide insight into the origin of the Fano response in a hybrid dielectric–metal structure.

Funding. Program Penelitian Dasar Unggulan Perguruan Tinggi DIKTI 2020, Kementerian Riset Teknologi Dan Pendidikan Tinggi Republik Indonesia; Nederlandse Organisatie voor Wetenschappelijk Onderzoek (740.018.021).

Acknowledgment. M.N. and A.A.I. acknowledge the support from the Ministry of Research and Technology, Indonesia. R.N.S.S. acknowledges the support from NWO Start Up.

Disclosures. The authors declare no conflicts of interest.

REFERENCES

1. B. Luk'yanchuk, N. I. Zheludev, S. A. Maier, N. J. Halas, P. Nordlander, H. Giessen, and C. T. Chong, "The Fano resonance in plasmonic nanostructures and metamaterials," Nat. Mater. **9**, 707–715 (2010).
2. M. F. Limonov, M. V. Rybin, A. N. Poddubny, and Y. S. Kivshar, "Fano resonances in photonics," Nat. Photonics **11**, 543–554 (2017).
3. A. E. Miroshnichenko, S. Flach, and Y. S. Kivshar, "Fano resonances in nanoscale structures," Rev. Mod. Phys. **82**, 2257–2298 (2010).
4. J.-H. Wu, J.-Y. Gao, J.-H. Xu, L. Silvestri, M. Artoni, G. C. La Rocca, and F. Bassani, "Ultrafast all optical switching via tunable Fano interference," Phys. Rev. Lett. **95**, 057401 (2005).
5. K. Nozaki, A. Shinya, S. Matsuo, T. Sato, E. Kuramochi, and M. Notomi, "Ultralow-energy and high-contrast all-optical switch involving Fano resonance based on coupled photonic crystal nanocavities," Opt. Express **21**, 11877–11888 (2013).
6. L. Stern, M. Grajower, and U. Levy, "Fano resonances and all-optical switching in a resonantly coupled plasmonic–atomic system," Nat. Commun. **5**, 4865 (2014).
7. F. Hao, P. Nordlander, Y. Sonnefraud, P. V. Dorpe, and S. A. Maier, "Tunability of subradiant dipolar and Fano-type plasmon resonances in metallic ring/disk cavities: implications for nanoscale optical sensing," ACS Nano **3**, 643–652 (2009).
8. J. Wang, C. Fan, J. He, P. Ding, E. Liang, and Q. Xue, "Double Fano resonances due to interplay of electric and magnetic plasmon modes in planar plasmonic structure with high sensing sensitivity," Opt. Express **21**, 2236–2244 (2013).
9. N. S. King, L. Liu, X. Yang, B. Cerjan, H. O. Everitt, P. Nordlander, and N. J. Halas, "Fano resonant aluminum nanoclusters for plasmonic colorimetric sensing," ACS Nano **9**, 10628–10636 (2015).
10. Y.-T. Chen, Y.-Y. Liao, C.-C. Chen, H.-H. Hsiao, and J.-J. Huang, "Surface plasmons coupled two-dimensional photonic crystal biosensors for Epstein-Barr virus protein detection," Sens. Actuators B **291**, 81–88 (2019).
11. J. Ye, F. Wen, H. Sobhani, J. B. Lassiter, P. Van Dorpe, P. Nordlander, and N. J. Halas, "Plasmonic nanoclusters: near field properties of the Fano resonance interrogated with SERS," Nano Lett. **12**, 1660–1667 (2012).

12. Z. Zhu, B. Bai, O. You, Q. Li, and S. Fan, "Fano resonance boosted cascaded optical field enhancement in a plasmonic nanoparticle-in-cavity nanoantenna array and its SERS application," Light Sci. Appl. **4**, e296 (2015).
13. H. Sun, S. Gong, Y. Niu, S. Jin, R. Li, and Z. Xu, "Enhancing Kerr nonlinearity in an asymmetric double quantum well via Fano interference," Phys. Rev. B **74**, 155314 (2006).
14. G. F. Walsh and L. Dal Negro, "Enhanced second harmonic generation by photonic–plasmonic Fano-type coupling in nanoplasmonic arrays," Nano Lett. **13**, 3111–3117 (2013).
15. B. Hopkins, A. N. Poddubny, A. E. Miroshnichenko, and Y. S. Kivshar, "Circular dichroism induced by Fano resonances in planar chiral oligomers," Laser Photon. Rev. **10**, 137–146 (2016).
16. L. Hu, Y. Huang, L. Fang, G. Chen, H. Wei, and Y. Fang, "Fano resonance assisting plasmonic circular dichroism from nanorice heterodimers for extrinsic chirality," Sci. Rep. **5**, 16069 (2015).
17. A. G. Lamprianidis and A. E. Miroshnichenko, "Excitation of nonradiating magnetic anapole states with azimuthally polarized vector beams," Beilstein J. Nanotechnol. **9**, 1478–1490 (2018).
18. B. Gallinet and O. J. F. Martin, "Ab initio theory of Fano resonances in plasmonic nanostructures and metamaterials," Phys. Rev. B **83**, 235427 (2011).
19. B. Gallinet and O. J. F. Martin, "Influence of electromagnetic interactions on the line shape of plasmonic Fano resonances," ACS Nano **5**, 8999–9008 (2011).
20. V. A. Tamma, J.-H. Lee, Q. Wu, and W. Park, "Visible frequency magnetic activity in silver nanocluster metamaterial," Appl. Opt. **49**, A11–A17 (2010).
21. Y. A. Urzhumov, G. Shvets, J. Fan, F. Capasso, D. Brandl, and P. Nordlander, "Plasmonic nanoclusters: a path towards negative-index metafluids," Opt. Express **15**, 14129–14145 (2007).
22. H.-H. Hsiao, Y. H. Chen, R. J. Lin, P. C. Wu, S. Wang, B. H. Chen, and D. P. Tsai, "Integrated resonant unit of metasurfaces for broadband efficiency and phase manipulation," Adv. Opt. Mater. **6**, 1800031 (2018).
23. J. Yang, C. Sauvan, H. T. Liu, and P. Lalanne, "Theory of fishnet negative-index optical metamaterials," Phys. Rev. Lett. **107**, 043903 (2011).
24. D. Dregely, M. Hentschel, and H. Giessen, "Excitation and tuning of higher-order Fano resonances in plasmonic oligomer clusters," ACS Nano **5**, 8202–8211 (2011).
25. B. Hopkins, A. N. Poddubny, A. E. Miroshnichenko, and Y. S. Kivshar, "Revisiting the physics of Fano resonances for nanoparticle oligomers," Phys. Rev. A **88**, 053819 (2013).
26. D. Punj, R. Regmi, A. Devilez, R. Plauchu, S. B. Moparthi, B. Stout, N. Bonod, H. Rigneault, and J. Wenger, "Self-assembled nanoparticle dimer antennas for plasmonic-enhanced single-molecule fluorescence detection at micromolar concentrations," ACS Photon. **2**, 1099–1107 (2015).
27. Z. Nie, A. Petukhova, and E. Kumacheva, "Properties and emerging applications of self-assembled structures made from inorganic nanoparticles," Nat. Nanotechnol. **5**, 15–25 (2010).
28. M. I. Mishchenko and L. D. Travis, "T-matrix computations of light scattering by large spheroidal particles," Opt. Commun. **109**, 16–21 (1994).
29. S. Mühlig, C. Menzel, C. Rockstuhl, and F. Lederer, "Multipole analysis of meta-atoms," Metamaterials **5**, 64–73 (2011).
30. C. F. Bohren and D. R. Huffman, *Absorption and Scattering of Light by Small Particles* (Wiley, 1983).
31. G. Gouesbet, "T-matrix formulation and generalized Lorenz–Mie theories in spherical coordinates," Opt. Commun. **283**, 517–521 (2010).
32. M. I. Mishchenko, L. D. Travis, and D. W. Mackowski, "T-matrix computations of light scattering by nonspherical particles: a review," J. Quant. Spectrosc. Radiat. Transf. **55**, 535–575 (1996).
33. M. Fruhnert, I. Fernandez-Corbaton, V. Yannopapas, and C. Rockstuhl, "Computing the T-matrix of a scattering object with multiple plane wave illuminations," Beilstein J. Nanotechnol. **8**, 614–626 (2017).
34. B. Wang, L.-L. Wang, and Z. Xie, "Accurate calculation of spherical and vector spherical harmonic expansions via spectral element grids," Adv. Comput. Math. **44**, 951–985 (2018).
35. R. N. S. Suryadharma, M. Fruhnert, C. Rockstuhl, and I. Fernandez-Corbaton, "Singular-value decomposition for electromagnetic-scattering analysis," Phys. Rev. A **95**, 053834 (2017).
36. O. R. Cruzan, "Translational addition theorems for spherical vector wave functions," Q. Appl. Math. **20**, 33–40 (1962).
37. S. Stein, "Addition theorems for spherical wave functions," Q. Appl. Math. **19**, 15–24 (1961).
38. Y.-L. Xu, "Calculation of the addition coefficients in electromagnetic multisphere-scattering theory," J. Comput. Phys. **127**, 285–298 (1996).
39. Y.-L. Xu, "Electromagnetic scattering by an aggregate of spheres: far field," Appl. Opt. **36**, 9496–9508 (1997).
40. D. W. Mackowski and M. I. Mishchenko, "Calculation of the T-matrix and the scattering matrix for ensemble of spheres," J. Opt. Soc. Am. A **13**, 2266–2278 (1967).
41. M. I. Mishchenko, L. D. Travis, and A. A. Lacis, *Scattering, Absorption, and Emission of Light by Small Particles* (Cambridge University, 2002).
42. Y.-L. Xu, "Electromagnetic scattering by an aggregate of spheres," Appl. Opt. **34**, 4573–4588 (1995).
43. J. D'Errico, "Eigenshuffle," https://www.mathworks.com/matlabcentral/fileexchange/22885-eigenshuffle.
44. B. Hopkins, D. S. Filonov, S. B. Glybovski, and A. E. Miroshnichenko, "Hybridization and the origin of Fano resonances in symmetric nanoparticle trimers," Phys. Rev. B **92**, 045433 (2015).
45. P. B. Johnson and R. W. Christy, "Optical constants of the noble metals," Phys. Rev. B **6**, 4370–4379 (1972).
46. D. E. Aspnes and A. A. Studna, "Dielectric functions and optical parameters of Si, Ge, GaP, GaAs, GaSb, InP, InAs, and InSb from 1.5 to 6.0 eV," Phys. Rev. B **27**, 985–1009 (1983).
47. R. N. S. Suryadharma, M. Fruhnert, I. Fernandez-Corbaton, and C. Rockstuhl, "Studying plasmonic resonance modes of hierarchical self-assembled meta-atoms based on their transfer matrix," Phys. Rev. B **96**, 045406 (2017).
48. R. N. S. Suryadharma, C. Rockstuhl, O. J. F. Martin, and I. Fernandez-Corbaton, "Quantifying Fano properties in self-assembled metamaterials," Phys. Rev. B **99**, 195416 (2017).